Available online at www.sciencedirect.com
SCIENCE DIRECT
Catalysis Today 107–108 (2005) 215–222
CATALYSIS TODAY
www.elsevier.com/locate/cattod

Characterization of Al–Cu and Al–Cu–Mg mixed oxides and their catalytic activity in dehydrogenation of 2-octanol

Mónica Crivello [a,*], Celso Pérez [a], Eduardo Herrero [a,*], Guillermo Ghione [a], Sandra Casuscelli [a], Enrique Rodríguez-Castellón [b]

[a] Centro de Investigación y Tecnología Química (CITeQ), UTN-FRC, Maestro López y Cruz Roja Argentina, 5016 Córdoba, Argentina
[b] Departamento de Química Inorgánica, Universidad de Málaga, Campus de Teatinos s/n, 29071 Málaga, Spain

Available online 3 October 2005

Abstract

Hydrotalcite (HT) type materials with different Cu:Mg:Al ratios were prepared. The samples were calcined at 450 °C and when the layered structure was destroyed mixed oxides were formed. Such oxides were reduced under a flow of hydrogen gas at 300 °C and their catalytic activity in dehydrogenation of 2-octanol was studied. High conversion and selectivity towards 2-octanone was observed. The samples without copper showed low conversion, but it increased with the copper content. The characterization of both precursors and reduced catalysts was carried out by XRD, XPS and diffuse reflectance. In the calcined samples, the XPS analysis detected Cu^{2+} in a $CuAl_2O_4$ spinel-like environment as well as CuO, while the reduced samples contained Cu^0 and copper ions, such as Cu^{2+} and Cu^+. Diffuse reflectance showed that the copper was present in two forms, the perfect and distorted octahedra. In the Al–Cu–Mg system, the copper was present in a cluster-like or bulk-like species, excepting the samples having a copper excess, where a spinel-like species was detected. By XRD, a greater structural ordering was observed in the samples containing a ratio $Cu^{2+}/Mg^{2+} \leq 1$ (Cu < 50% keeping in mind only cations M^{2+}) and in those having a ratio ($M^{3+}/M^{3+} + M^{2+}$) approximately equal to 0.25; in this case other species were not detected.
© 2005 Elsevier B.V. All rights reserved.

Keywords: Layered double hydroxides; Hydrotalcites; Alcohols dehydrogenation; Mixed oxides; Octanol decomposition

1. Introduction

Layered double hydroxides (LDH) or hydrotalcite-like compounds (HLC) have recently received much attention [1] in view of their potential usefulness as adsorbents, anion exchangers, and most importantly as basic catalysts [2–6]. These compounds are represented by the formula $(M_{(1-x)}^{2+}M_x^{3+}(OH)_2)^{x+}(A_{x/n}^{n-}mH_2O)^{x-}$, where the divalent ion may be Mg^{2+}, Cu^{2+}, Zn^{2+}, Ni^{2+}, and the trivalent ion Al^{3+}, Fe^{3+}, Cr^{3+}. The compensating anions may be CO_3^{2-}, OH^-, SO_4^{2-}, NO_3^-, Cl^-, and x can have values between 0.25 and 0.33 [7]. It is an alternating layered structure with positively charged brucite-like layers ($M^{2+}M^{3+}(OH)$), where M^{2+} cations are substituted by M^{3+} cations and interlayers contain the charge balancing anions and water molecules.

Numerous studies on the physico-chemical properties and thermal stability of various LDH have been reported [8–11]. Upon thermal decomposition, a highly active homogeneous mixed oxide is obtained from these materials at about 450 °C, which is potentially a basic catalyst for a variety of organic transformations, such as aldol condensations [12,13], epoxidation of limonene [14], alkylation of phenol [15], epoxidation of activated olefins with hydrogen peroxide [16], catalytic transfer hydrogenation of citral [17], partial oxidation of methane to synthesis gas [18], oxidative methanol reforming [19,20].

The aldehydes of 8–13 atoms of carbon are used in the perfumery industry [21], specifically the 2-octanone is used in perfumes and colognes in low concentrations and in

* Corresponding authors. Tel.: +54 351 469 05 85; fax: +54 351 469 05 85.
E-mail addresses: mcrivello@scdt.frc.utn.edu.ar (M. Crivello), eherrero@scdt.frc.utn.edu.ar (E. Herrero).

0920-5861/$ – see front matter © 2005 Elsevier B.V. All rights reserved.
doi:10.1016/j.cattod.2005.07.168

artificial citric oils. The classic method to oxidize primary alcohols uses chromic acid as the agent oxidizer, generating a great quantity of polluting effluent. For a better protection of the environment, it is desirable to find solid bases which would substitute liquid catalysts and would also show all the advantages of heterogeneous catalysis, i.e. ease of separation of the products, decreased corrosion of the reactor, and possible regeneration of the catalyst. Some aldehydes used in perfumery are obtained by dehydrogenation of the corresponding alcohol in gas phase [22]. LDH or HLC constitute a special class of inorganic materials, which have aroused a lot of interest in the last years, particularly for use in the reaction of catalytic dehydrogenation of alcohols [3,23]. The copper incorporation in the LDH showed interesting results in the conversion and selectivity of the reaction under study.

In this work, the influence of copper on the structural and catalytic properties of the samples was studied. The precursors, the mixed oxides and the samples reduced have been characterized by different physico-chemical methods, such as X-ray powdered diffraction (XRD), infrared (FT-IR), X-ray photoelectron spectroscopy (XPS), diffuse reflectance UV–vis (DR), thermogravimetric analysis (TGA), differential thermal analysis (DTA) and determination of specific surface area.

The catalytic performance of the mixed oxides obtained at 450 °C and reduced with hydrogen at 300 °C in dehydrogenation of 2-octanol is also reported.

2. Experimental

2.1. Samples preparation

Samples have been prepared [24], changing the M^{2+}/Al^{3+} and the Cu^{2+}/Mg^{2+} molar ratios, in order to assess the effect of these variables on the properties of the HLC and their calcination products.

The synthesis procedure was as follows: two solutions were prepared, A and B. The aqueous solutions of $Mg(NO_3)_2{\cdot}6H_2O$, $Cu(NO_3)_2{\cdot}3H_2O$ and $Al(NO_3)_3{\cdot}9H_2O$ (solution A) (1.5 mol), while the solution B, were prepared dissolving 0.1 mol Na_2CO_3 and 0.33 NaOH in 150 ml distilled water. Then, both solutions were added simultaneously to 50 ml of water (60 ml/h). The addition was carried out at room temperature and the light-green suspension was continuously stirred magnetically, while pH was maintained at a value of 10 ± 0.2. The precipitate was aged in the mother liquor for 4 h at room temperature, and then it was separated by centrifugation at 2800 rpm; the solid was washed with bidistilled water until pH 7, and then was dried overnight at 90 °C in the open air. The solids were finally calcined in static air at 450 °C for 9 h. Hard bluish-green solids were obtained.

2.2. Sample characterization

The XRD powder patterns were collected on a Rigaku diffractometer, using monochromatized Cu Kα radiation ($\lambda = 1.54$ Å) at a scan speed of 1/4 min in 2θ and interfaced to a DACO-MP data acquisition microprocessor provided with Diffract/AT software. Thermogravimetric analysis was carried out on an Setaram instrumentation apparatus. Samples (ca. 30 mg) were loaded and heated under a flow of synthetic air and at a heating rate of 10 °C/min to 600 °C. Diffuse reflectance UV–vis-near infrared spectra were obtained using a spectrophotometer Shimadzu 8100 and $BaSO_4$ as reference. X-ray photoelectron spectroscopy (XPS) analyses were carried out using a Physical Electronics PHI 5700 spectrometer with a non-monochromatic Mg Kα radiation (300 W, 15 kV, 1253.6 eV) as the excitation source. High-resolution spectra were recorded in the constant pass energy mode at 29.35 eV, using a 720 mm diameter analysis area. Under these conditions, the Au $4f_{7/2}$ line was recorded with 1.16 eV FWHM at a binding energy of 84.0 eV. The spectrometer energy scale was calibrated using Cu $2p_{3/2}$, Ag $3d_{5/2}$ and Au $4f_{7/2}$ photoelectron lines at 932.7, 368.3 and 84.0 eV, respectively. Charge referencing was done against adventitious carbon (C 1s, 284.8 eV). The pressure in the analysis chamber was maintained lower than 5×10^{-6} Pa. PHI ACCESS ESCA-V6.0 F software package was used for acquisition and data analysis. A Shirley-type background was subtracted from the signals. Specific surface area was determined by the BET method, which was recorded on a Micromeritics ASAP 2000 instrument. The precursors were degassed at 200 °C and the calcined materials at 390 °C, both for 50 min. The Fourier transform-infrared spectra (FT-IR) of the samples were recorded on a Jasco FT/IR 5300 apparatus, with a nominal resolution of 4 cm^{-1} and 16 scans; the sample was pressed in KBr pellets.

Table 1
Chemical composition of the LDH studied

LDH	M^{2+}	$Al^{3+}/Al^{3+} + M^{2+}$	M^{2+}/Al^{3+}	Cu^{2+}/Mg^{2+}	% Cu (only M^{2+})
HT_0	Mg	0.25	3.00	–	0
HT_{38}	Cu–Mg	0.14	6.14	0.71	38.4
HT_{47}	Cu–Mg	0.25	3.00	0.90	47.3
HT_{60}	Cu–Mg	0.18	4.55	1.33	60.1
HT_{80}	Cu–Mg	0.25	3.00	3.91	79.7
HT_{100}	Cu	0.25	3.00	–	100

2.3. Catalytic activity

Catalytic runs were performed in a home-made system formed by a tubular glass flow reactor (10 mm external diameter). The temperature of the reactor was measured by a thermocouple placed in the middle of the catalyst bed. The reactions were conducted at atmospheric pressure and reaction temperatures at 300 °C. The LDH was calcined at 450 °C for 9 h and before the start of the experiment the samples were reduced under a flow of hydrogen gas at 300 °C for 2 h. The reagent was 2-octanol (Anedra, 97%) and was introduced in the reactor through a positive displacement pump (W/F = 21.2 g h/mol). Liquid products were condensed and samples were taken each 30 min up to arrive to a time on stream of 240 min. The reaction mixture was analyzed by a Hewlett-Packard 5890 gas chromatography equipped with a DB-1 (J&W Scientific) column and TCD detector.

3. Results and discussion

3.1. Chemical composition

Table 1 gives the composition of the LDH studied. As can be seen, the ($Al^{3+}/Al^{3+} + M^{2+}$), Cu^{2+}/Mg^{2+} molar ratio and % Cu (keeping in mind only cations M^{2+}) were changing.

3.2. X-ray diffraction

For X-rays diffraction, in all cases the hydrotalcite phase was detected, including the sample without magnesium (HT_{100}). Fig. 1 compares the XRD patterns for three LDH prepared with different ($Al^{3+}/Al^{3+} + M^{2+}$) and Cu^{2+}/Mg^{2+} molar ratio. As can be seen, the three precursors possess the typical structure with stacked layers similar to those found by Reichle et al. [25], although in the HT_{60} phase malachite and in the HT_{38} another non-identified phases was observed. This coincides with the variation in the relationship M^{2+}/Al^{3+}. In the HT_{60} and HT_{38}, the relationship M^{2+}/Al^{3+} is above to three, with excess of Cu^{2+} in the first case and of Mg^{2+} in the second. On the other hand, and for a given series of samples, sharpness of the peaks (directly related to crystallinity) decreases as the relative content of Cu in the sample increases.

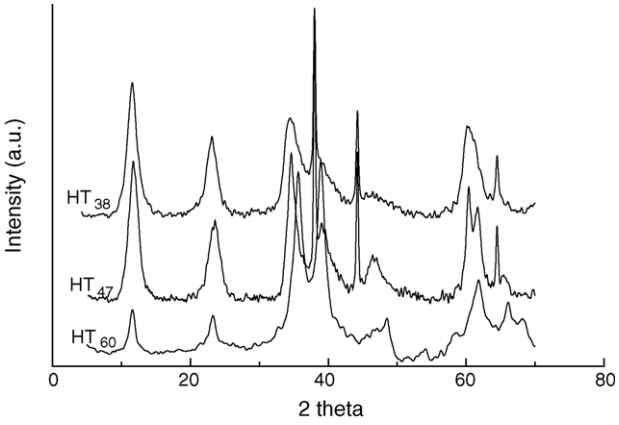

Fig. 1. XRD patterns for different LDH.

The lattice parameters for the samples studied have been included in Table 2. Parameter *a* has been calculated as twice the spacing of the peak corresponding to diffraction by planes (1 1 0) [1], while parameter *c* is calculated from the position of the first, intense, basal, peak (plane 0 0 3 if hexagonal packing is assumed) and $c = 3d_{(0\ 0\ 3)}$.

The *d*-spacing for planes (0 0 3) for a hexagonal packing is in the range of 7.56–7.65 Å for all samples. Assuming a value of 4.8 Å for the width of a brucite layer [26], the interlayer space is 2.76–2.85 Å.

Magnesium/copper substitution in the brucite-like layers does not give rise to deep changes in the *a* parameter, as the ionic radii of both cations are rather similar (0.86 Å for Mg^{2+} and 0.87 Å for Cu^{2+} in octahedral coordination), and thus the *a* parameter is in the range of 3.06–3.08 Å for all samples.

Heating the precursors at 450 °C destroyed the layered structure and a MgO and CuO phase were observed. Table 2 shows the different species detected by XRD in the precursors as in the samples after calcined. After the reduction, it was observed that in all cases the Cu^{2+} change to Cu^0, except in the HT_{60} where Cu^+ and Cu^0 were detected.

3.3. UV–vis diffuse reflectance (DR) spectroscopy

In Fig. 2, the spectra of the uncalcined and calcined HT_{100} (LDH CuAl) are shown. The UV–vis DR spectra of the uncalcined sample show two main bands; one between 260 and 400 nm and an other around 700 nm together with a shoulder. Both bands were typical copper–aluminum samples. The band around 240 nm can be attributed to

Table 2
Different species detected by DRX in the precursor and in the calcined samples

LDH	Species precursors	*c*	*a*	Species calcined samples	S_{BET} (m^2/g)
HT_0	HT	22.86	3.06	MgO	217
HT_{38}	HT + non-identified phase	22.95	3.07	CuO–MgO	120
HT_{47}	HT	22.68	3.06	CuO–MgO	156
HT_{60}	HT + Ma	22.71	3.08	CuO–traces of MgO	125
HT_{100}	HT	22.71	3.08	CuO	35

HT, hydrotalcite; Ma, malachite.

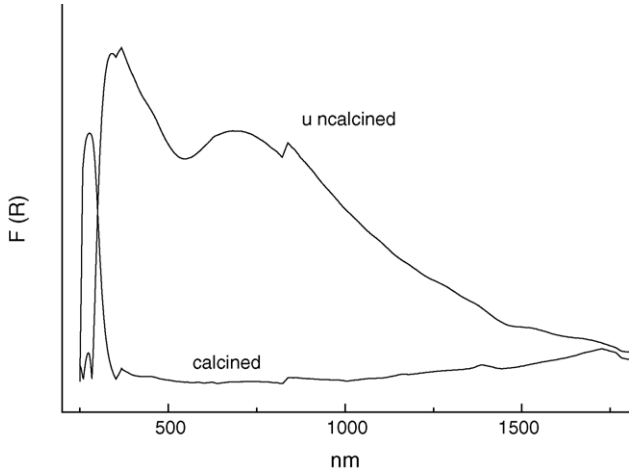

Fig. 2. UV–vis diffuse reflectance spectra of uncalcined and calcined LDH CuAl.

the $O^{2-} \rightarrow Cu^{2+}$ ligand to metal charge transfer transition. The band at 680 nm can be attributed to the transition of Cu^{2+} ions in the distorted octahedron [27] and the shoulder that appears at 838 nm is attributed to the transition of the Cu^{2+} in symmetry octahedral.

The UV–vis DR spectra of the calcined sample presents only one a band around 260 nm that is characteristic of copper–aluminum samples and has been attributed to the $^2Eg \rightarrow {}^2T_2g$ spin-allowed transition of Cu^{2+} ions in the distorted octahedral environment with a spinel-type structure.

The UV–vis DR spectra of the uncalcined sample LDH CuMgAl with different Cu^{2+}/Mg^{2+} molar ratio were shown in Fig. 3. These samples exhibit a band around 700 nm which can be attributed to transition of Cu^{2+} in the distorted octahedron. When comparing this band in the three spectra, it is observed that it is plane in the case of the HT_{60} and lightly displaced to a shorter length of wave, which would indicate a bigger distortion of the octahedron. In this case, the relationship Cu^{2+}/Mg^{2+} is of 1.33 (excess of Cu^{2+}). The shoulder that is present at 838 nm is attributed to the transition of the Cu^{2+} in symmetry octahedral (smaller in HT_{60}). The band at 260 nm, displaced in the HT_{60} toward a greater length of wave, is due to a $O^{2-} \rightarrow Cu^{2+}$ charge transfer process. The band around 330 nm (as shoulder in HT_{60}) is attributed to the increment of the lateral interaction of the ions Cu^{2+} with Al^{3+} [28].

The UV–vis DR spectra of the calcined sample (Fig. 3) exhibit a broad band between 300 and 350 nm together with a shoulder superimposed on the band between 600 and 800 nm. These bands are attributed to the charge transfer involving Cu^{2+}–O^{2-}–Cu^{2+} species, possibly cluster-like or bulk-like species. The exception is present in the HT_{60} where a great band is observed around 280 nm and a plane band with two shoulders at 368 and 838 nm, characteristic of the aluminium–copper samples. These bands have been attributed to the $^2Eg \rightarrow {}^2T_2g$ spin-allowed the transition of Cu^{2+}.

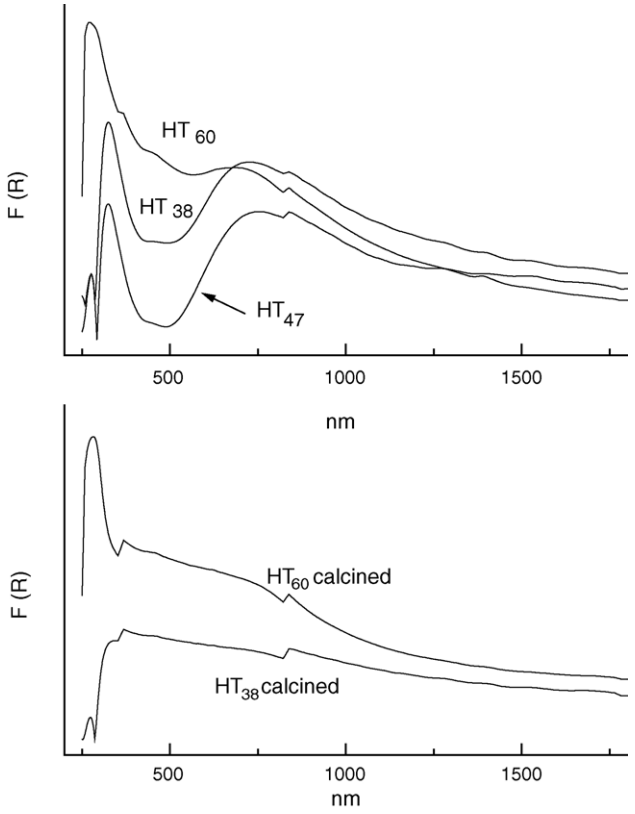

Fig. 3. UV–vis diffuse reflectance spectra of LDH CuMgAl with different Cu^{2+}/Mg^{2+} molar ratio.

3.4. XPS analysis

The nature of the species active present on the surface is important for establishing the properties of the catalyst. To this purpose, the XPS analysis has been done in order to obtain information about the surface composition of the Cu–Mg–Al mixed oxides derived from hydrotalcite-like samples. The relative concentration at the surface has been evaluated by XPS in both calcined and H_2-reduced samples. The surface Cu/M (M = Mg, Al) atomic ratios, summarized in Table 3, have been calculated from peak areas, considering photoelectron cross sections and mean free paths. There is overlapping of both Cu 3s–Al 2s and Cu 3p–Al 2p core levels. Due to the overlapping of Cu 3p and Al 2p core level peaks, a deconvolution of both contributions was

Table 3
Relative concentration of the surface evaluated by XPS, in calcined and reduced samples

LDH	Treatment	$(Cu/Mg)_{at}$	$(Cu/Al)_{at}$	$(Cu/Mg + Al)_{at}$
HT_{60}	Calcined at 450 °C	0.80	1.32	0.50
HT_{38}	Calcined at 450 °C	0.79	1.72	0.54
HT_{47}	Calcined at 450 °C	0.65	0.75	0.34
HT_{60}	Reduced at 300 °C	0.36	0.53	0.21
HT_{38}	Reduced at 300 °C	0.39	0.51	0.22
HT_{47}	Reduced at 300 °C	1.15	0.99	0.53

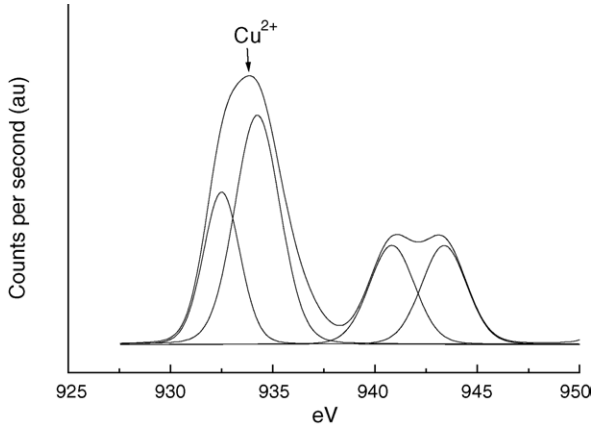

Fig. 4. Central level Cu $2p_{3/2}$ of the calcined HT_{60} sample and two deconvolution components.

carried out to quantitatively determine the Al 2p peak intensity. The largest copper concentration at the surface is observed in the HT_{38} calcined sample. The decrease of the Cu/Mg and Cu/Al intensity ratio in H_2-reduced HT_{60} and HT_{38} samples clearly indicates a lack of copper dispersion as a consequence of Cu particle formation from the phase where Cu^{2+} is dispersed on oxide. When the relationship $M^{2+}/Al^{3+} = 3$ and $Cu^{2+}/Mg^{2+} < 1$, the biggest concentration of superficial copper is observed.

Figs. 4 and 5 show the Cu $2p_{3/2}$ peaks of the HT_{60} calcined and hydrogen reduced samples, respectively. From these spectra it is evident that the line profile changes drastically after hydrogen reduction at 300 °C. The calcined sample presents the principal Cu $2p_{3/2}$ peak around 934 eV, which is characteristic of Cu^{2+} species [29], when referenced to the C 1s core level at 285.0 eV. An additional means of identifying Cu^{2+} ions is the satellite line of the principal, whose origin is complex and has been explained as due to electron shake-up processes [30], final state effects [31], and charge transfer mechanisms. Such peaks have been deconvoluted into two contributions centered around 932.5 and 934.2 eV. The latter peak can be attributed to Cu^{2+} in a $CuAl_2O_4$ spinel-like environment, whereas the peak at 932.5 eV is attributed to Cu^{2+} in CuO. When the peak of oxygen was deconvoluted, a single peak was shown around 531 eV which is attributed to oxides, except in the HT_{60} where another species are detected (possibly spinel-like).

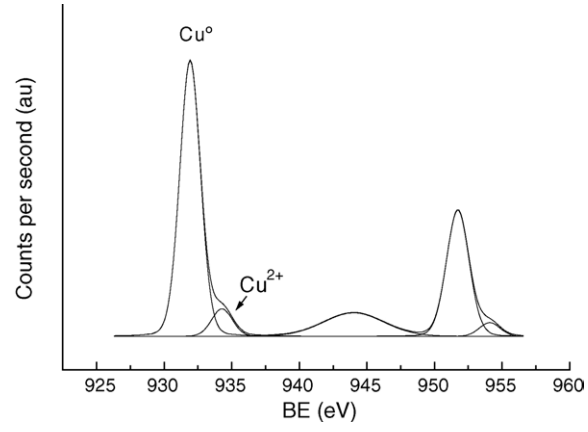

Fig. 5. Central level Cu $2p_{3/2}$ of the reduced HT_{60} sample.

Fig. 5 shows the spectra of HT_{60} H_2-reduced sample. As in the other analyzed cases, the almost total disappearance of the satellite peak and the simultaneous shift of the principal Cu $2p_{3/2}$ peak towards lower binding energy upon H_2 reduction at 300 °C, show that after reduction, the copper species are Cu^+, Cu^0 and some Cu^{2+}.

3.5. Thermal analyses (TGA and DTA)

Thermal properties of the sample have been assessed by DTA and TGA. These studies were carried out in air. The curves recorded for samples HT_{60}, HT_{38} and HT_{47} are shown in Fig. 6. Several peaks were observed, the first at approximately to 200 °C, due to the loss of water, showing in this case two minima, at an approximate temperature of 180 °C (HT_{60} and HT_{38}) when the relationship was $M^{2+}/M^{3+} > 3$ and at 210 °C when the relationship was $M^{2+}/M^{3+} = 3$ (HT_{47}). The third at 400 °C is generally attributed to the removal of water (from the layer hydroxyl groups) and of carbon dioxide (from interlayer carbonate anions). It can be observed that in HT_{38} (excess of Mg^{2+}) this peak is more marked that in the other LDH and in HT_{60} (excess of Cu^{2+}), this peak is very weak. In all cases, a peak at 300 °C was detected, this can be due to the formation of amorphous alumina species that is not detected by XRD.

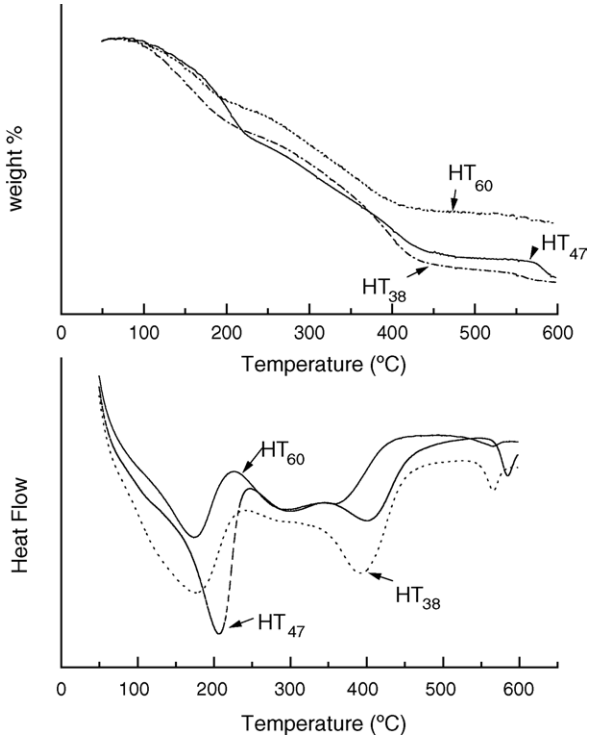

Fig. 6. Differential thermal analysis and thermogravimetry curves of Cu–Mg–Al samples HT_{47}, HT_{38} and HT_{60}.

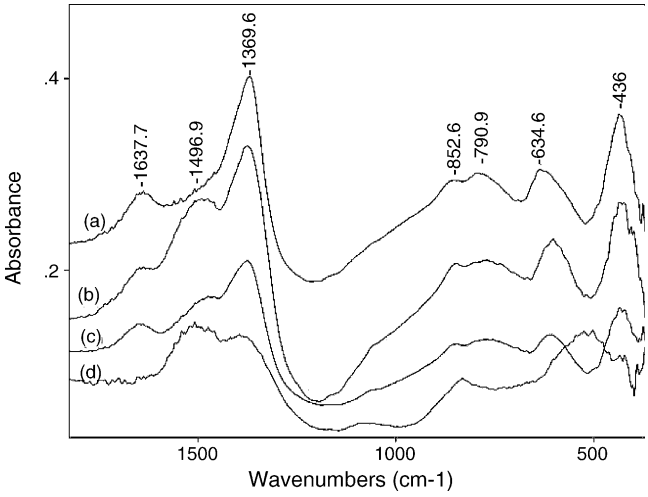

Fig. 7. FT-IR spectrum of samples with different content of copper: (a) HT_{47}, (b) HT_{60}, (c) HT_{38} and (d) HT_{100}.

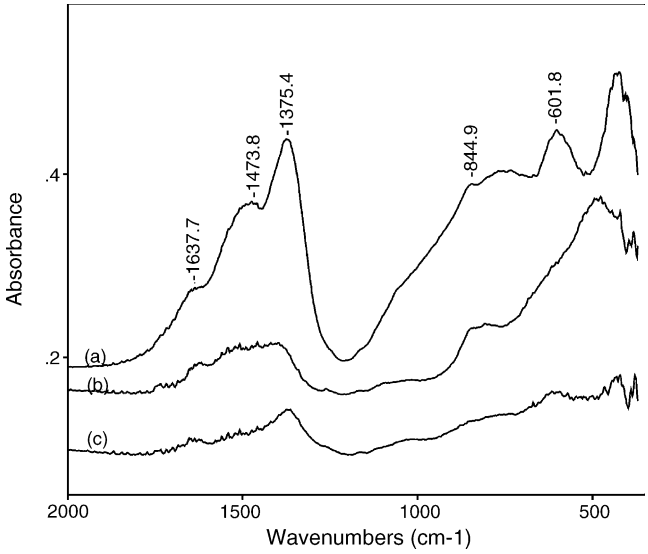

Fig. 8. FT-IR spectrum of sample HT_{60}: (a) uncalcined, (b) calcined and (c) reduced.

In the case of the analyses of TGA, two consecutive weight losses are recorded, as expected for hydrotalcite-like compounds with vaporizable interlayer anions. The first weight loss between 50 and 200 °C can be attributed to the removal of interlayer water and the liberation of the molecular water located in the galleries of the LDH. The second in the range of 250–430 °C, is attributed to the removal of water and carbon dioxide and give place to the formation of metallic oxides.

3.6. FT-IR spectroscopy

Further evidence of the characterization of the samples prepared has been obtained from the FT-IR spectra of the samples. These are very similar in all cases, except in the HT_{100}, and the main features arise in the interlayer anion and in the water molecules. The spectrum for samples HT_{100}, HT_{60}, HT_{38} and HT_{47} are given in Fig. 7. The main absorption at about 3450 cm^{-1} (part not shown in this figure) is due to the OH stretching mode of hydroxyl groups, both in the interlayer water molecules and in the hydroxyls in the layers. The extended absorption in the low wavenumbers side of this band has been recorded in some cases as a broad shoulder around 3100–3050 cm^{-1} and it has been ascribed [32] to water molecules hydrogen-bonded to interlayer carbonate anions. The rather weak absorption at 1637 cm^{-1} (except in HT_{100}) is due to the deformation mode of interlayer water molecules. The band at 1369 cm^{-1}, with a shoulder at 1496 cm^{-1} (this shoulder is not observed in HT_{47}), is due to mode ν_3 of carbonate species. Although, this is a single vibration, triply degenerated mode, it splits into two bands due to a lowering in the local symmetry of the carbonate anion in the interlayer space, because of electrostatic interaction either with the positively charged layers, or with the water molecules. The extremely weak shoulder at 1061 cm^{-1} (not observed in same samples) is due to the ν_1 mode of carbonate which, although originally forbidden for the D_{3h} symmetry of the free ion, becomes activated upon a reduction in its symmetry, probably by hydrogen bonding to interlayer water molecules and layer OH groups. Finally, the bands recorded at 852, 790, 634 and 436 cm^{-1} (very weak in HT_{100}) are due to lattice vibrations involving the layer cations (Mg^{2+}, Cu^{2+}, and Al^{3+}).

The spectra of the HT_{60} uncalcined, calcined and reduced sample is shown in Fig. 8. The spectra of calcined and reduced samples showed only strong absorptions in the low wavenumbers range, due to lattice metal–oxygen vibrations, and weak absorptions due to surface weakly adsorbed water molecules.

3.7. Measurement of specific surface areas

The specific surface area was determined by the BET method. The values obtained are summarized in Table 2. This shows that the biggest area was obtained in the HT_{47} (good relationship), while in the sample without magnesium the area was of 35 m^2/g.

3.8. Catalytic activity

Catalytic activity of samples calcined at 450 °C and hydrogen reduced at 300 °C was assessed in dehydrogenation of 2-octanol to 2-octanona, in some samples octenes and water were observed. The results obtained are summarized in Figs. 9 and 10. Several differences were found in the nature of the catalyst and its catalytic performance. As a general trend, although the sample without copper has low conversions, it increases with the copper content while that the presence of small percentages of magnesium gives the catalyst stability. The highest conversions were observed in samples with percentages of copper over and above 50%. Fig. 9 shows the variation of conversions and selectivity as a function of the copper content (the percentage was calculated keeping in

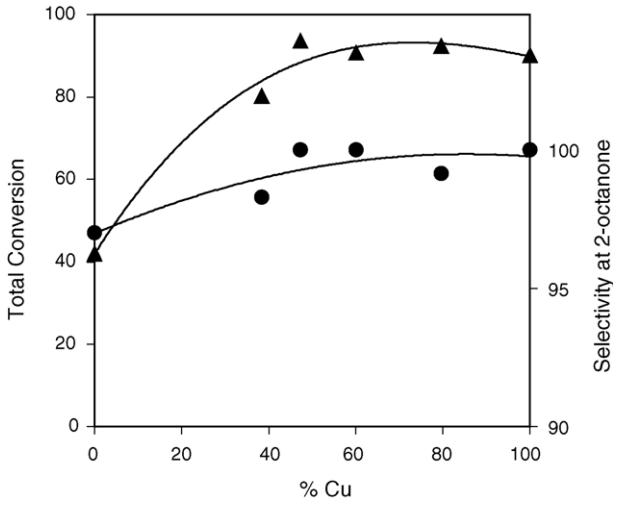

Fig. 9. Variation of the conversion and selectivity in relation to the copper content. Conversion (▲) and selectivity (●).

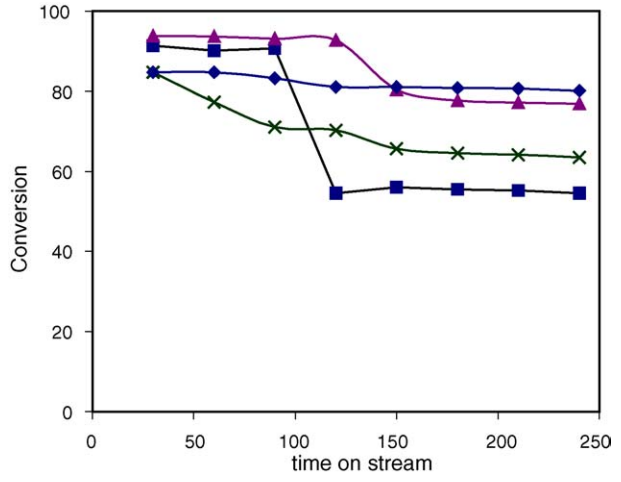

Fig. 10. Conversion vs. time on stream using catalysts with different content of magnesium. HT_{100} (■), HT_{38} (x), HT_{47} (▲) and HT_{60} (◆).

mind only the cations 2+). The selectivity to 2-octanona slightly increases with the increase in the copper content.

Fig. 10 shows the conversion versus time on stream using catalysts with different percentages of magnesium in its structure. As shown, initially the conversion was similar in all cases and remained unalterable, except in those samples without magnesium (HT_{100}), where the conversion falls abruptly after a short time of use. In the samples HT_{38} and HT_{47}, the conversion decrease only a 15%. The sample that presented higher stability was the HT_{60}.

4. Conclusions

Hydrotalcite-like materials containing Cu^{2+} and Mg^{2+} cations in the layers, together with Al^{3+}, and carbonate in the interlayer, have been prepared by a coprecipitation method, with different Cu/Mg/Al molar ratios.

These solids are transformed to mixed oxides when calcined at 450 °C, the layered structure being completely destroyed. The removal of water and carbon dioxide leads to an increase in the specific surface area of the solids; this value is related to the content of magnesium in the samples.

For diffraction of X-rays, in all cases the hydrotalcite phase was detected, including in the sample without magnesium. When the samples were calcined at 450 °C, MgO and CuO phase were observed.

In respect of the structure it was determined that, in the uncalcined samples the copper forms a perfect octahedron or a distorted octahedron. This distortion increases with the increase of copper in the sample. In calcined samples, two different species were detected, depending on the copper content in the sample. In the samples with a smaller quantity of copper, clusters-like or bulk-like species were detected, while in samples with a high content, the ions Cu^{2+} in a distorted octahedron environment of the aluminum surface with a spinel-type structure were detected.

The presence of the signal at 934.2 eV, observed by analysis of XPS, attributed to Cu^{2+} in environment spinel-type structure ($CuAl_2O_4$), justifies the appearance of Cu^{+} and Cu^{2+} in the reduced samples, since the copper that is in this structure is more difficult to reduce.

The synthesized catalysts show a high conversion and selectivity toward 2-octanona decreasing abruptly in the case of those catalysts without magnesium. The catalytic activity can also be attributed to the copper content in each sample, the best catalytic activities were presented in those whose percentage in copper was superior to 50%. It can be proposed that the presence of small percentages of magnesium contributes to a significant extent to the dispersion of entities of oxidized copper at the surface of the calcined samples.

Acknowledgement

Part of this work has been carried out in Málaga University under the direction of Dr. E. Rodríguez Castellón with an academic stay granted by CYTED.

References

[1] F. Cavani, F. Trifiro, A. Vaccari, Catal. Today 11 (1991) 173.
[2] W. Reichle, J. Catal. 94 (1985) 547.
[3] P. Hathaway, M. Davis, J. Catal. 116 (1989) 263.
[4] J. Roelofs, A. van Dillen, K. de Jong, Catal. Today 60 (2000) 297.
[5] V. Rives, O. Prieto, A. Dubey, S. Kannan, J. Catal. 220 (2003) 161.
[6] F. Prieto, D. Tichit, R. Teissier, B. Coq, Catal. Today 55 (2000) 103.
[7] W. Reichle, Chem. Technol. 1 (1986) 58.
[8] J. Theo Kloprogge, R. Frost, Appl. Catal. A 184 (1999) 61.
[9] F. Trifiro, A. Vaccari, O. Clause, Catal. Today 21 (1994) 185.
[10] G. Carja, R. Nakamura, T. Aida, H. Niiyama, J. Catal. 218 (2003) 104.
[11] J. Roelofs, A. van Dillen, K. Jong, Catal. Today 60 (2000) 297.
[12] J. Roelofs, D. Lensveld, A. van Dillen, K. Jong, J. Catal. 203 (2001) 184.

[13] K. Rao, M. Gravelle, J. Valente, F. Figueras, J. Catal. 173 (1998) 115.
[14] M. Aramendia, V. Borau, C. Jiménez, J. Luque, J. Marinas, J. Ruiz, F. Urbano, Appl. Catal. A 216 (2001) 257.
[15] S. Velu, C. Swamy, Appl. Catal. A 119 (1994) 241.
[16] C. Cativiela, F. Figueras, J. Fraile, J. Garcia, J. Mayoral, Tetrahedron Lett. 36 (1995) 4125.
[17] M. Aramendia, V. Borau, C. Jiménez, J. Marinas, J. Ruiz, F. Urbano, Appl. Catal. A 206 (2001) 95.
[18] H. Morioka, Y. Shimizu, M. Sukenobu, K. Ito, E. Tanabe, T. Shishido, K. Takehira, Appl. Catal. A 215 (2001) 11.
[19] S. Murcia-Mascarós, R. Navarro, L. Gómez-Sainero, U. Costantino, M. Nocchetti, J. Fierro, J. Catal. 198 (2001) 338.
[20] S. Velu, K. Suzuki, M. Okazaki, M. Kapoor, T. Osaki, F. Ohashi, J. Catal. 194 (2000) 373.
[21] K. Bauer, D. Garbe, H. Surburg, Common Fragances and Flavors Materials, 2nd ed., VCH, New York, 1990, p. 11.
[22] C. Chapuis, D. Jacob, Appl. Catal. A 221 (2001) 93.
[23] M. Crivello, C. Pérez, S. Casuscelli, J. Fernández, E. Herrero, Proceedings of XVII Simposio Iberoamericano de Catálise Porto, Portugal, 2000, p. 501.
[24] O. Clause, M. Gonçalves Coelho, M. Gazzana, D. Mateuzzi, F. Triffiro, A. Vaccari, Appl. Clay Sci. 8 (1993) 169.
[25] W. Reichle, S. Kang, D. Everhardt, J. Catal. 101 (1986) 352.
[26] C.F. Pérez, M.E. Crivello, O.A. Orio, J.D. Fernández, E.R. Herrero, S.G. Casuscelli, Proceedings of XVIII Simposio Iberoamericano de Catálisis, Isla Margarita, Venezuela, 2002, p. 275.
[27] S. Velu, K. Suzuki, M. Okazaki, M. Kapoor, T. Osaki, F. Ohashi, J. Catal. 194 (2000) 373.
[28] G. Centi, S. Perathoner, D. Biglino, E. Giamello, J. Catal. 152 (1995) 75.
[29] R. Figueiredo, A. Martínez Arias, M. López Granados, J.L. Fierro, J. Catal. 178 (1998) 146.
[30] K.S. Kim, J. Electron Spectrosc. Relat. Phenom. 3 (1974) 217.
[31] K. Okada, A. Kotani, J. Electron Spectrosc. Relat. Phenom. 86 (1997) 119.
[32] M. Holgado, V. Rives, M. San Román, Appl. Catal. 214 (2001) 219.